Searching for prompt and long-lived Axion-Like Particles decaying into hadrons at FCC-ee

Meena Meena *

Jeremy Andrea *, Eric Conte *, Auguste Besson *, Ziad El Bitar *, Gaelle Sadowski *

Abstract

This study explores the potential for Axion-Like Particles (ALPs) detection at the Future Circular Collider in its electron-positron phase (FCC-ee) using a fast simulation of the CLIC-like detector (CLD). The focus is on the hadronic decay of the ALP via a coupling to a gluon pair, a promising channel for new physics. A dedicated sensitivity analysis is performed in order to identify the region of parameter space (in terms of axion mass and couplings) accessible by the experimental setup. Both prompt and long-lived ALPs are considered in this analysis. The analysis is followed by a reinterpretation of the results in the context of another coupling basis and of benchmarks involving a non-null axion coupling to a photon pair. The presented analysis is still work in progress, and further improvements on event selection and signal extraction are being investigated. In particular important handles to improve the signal to background ratio have not been exploited yet.

1 Introduction

The Standard Model (SM) of particle physics is a well-established framework describing fundamental interactions. However, it fails to explain multiple phenomena such as existence of dark matter (DM), neutrino masses, and the baryon asymmetry of the universe (BAU). These unresolved questions motivate the search for physics beyond the SM (BSM), where new particles and interactions could provide crucial insights. One such proposed BSM particle, the Axion-Like Particle (ALP), naturally emerges in extensions of the SM that feature approximate global symmetry breaking, leading to the appearance of pseudo Nambu-Goldstone bosons. If the pseudo Nambu-Goldstone boson is a pseudoscalar, it is commonly referred to as an ALP. The concept of an axion was originally introduced by Peccei and Quinn in 1977 to address the problem of Charge-Parity violation in Quantum ChromoDynamics (strong $\not{C}\not{P}$) [1–4]. However, ALPs also appear in a broader range of BSM scenarios, including string theory, composite Higgs models, and various mechanisms of electroweak symmetry breaking (EWSB).

ALPs can also be long-lived ALPs or, in other terms, they can decay after traveling a large distance from their production point. The Long-lived particles (LLPs) have a unique discovery potential, as most of SM processes are prompt particles, making it easier to isolate potential BSM signals. Additionally, many well-motivated BSM scenarios predict LLPs, making them an attractive target for experimental exploration [5].

The Future Circular Collider in its electron-positron phase (FCC-ee) [6, 7] offers an unprecedented opportunity to explore BSM physics. In particular, the Tera-Z phase of FCC-ee will operate at the Z-pole, producing approximately 5×10^{12} Z bosons. This enormous dataset provides exceptional sensitivity to rare processes and new particle searches, including those involving LLPs [8, 9]. The long lifetime and exotic decay signatures of ALPs make them well-suited for detection in such high-statistics environments [10, 11].

*Université de Strasbourg, CNRS, IPHC UMR7178, F-67000 Strasbourg, France (meena.meena@cern.ch)

In this study, we focus on the production of a single axion (labeled ax in the following) in association with a photon at the FCC-ee, with the axion decaying into a pair of gluons. This analysis is complementary to the one devoted to the golden channel where the axion is decaying into a pair of photon. By leveraging the unique capabilities of the FCC-ee, this work aims to explore the discovery potential for axions and contribute to the broader search for BSM physics.

This paper is organised as follows. The first section is devoted to the description of the theoretical framework. Then, the signal process will be motivated in details and a first overview on the relevant region of parameter space will be highlighted. Afterwards, the procedure used for generating the Monte-Carlo samples will be explained and an emphasis will be placed on the detector simulation step. The next section will be dedicated to the analysis selection and the sensitivity study. It will be followed by a discussion about the possible reinterpretations of the study results. Finally, the main results will be summarised in the last section.

2 Theoretical Framework

The Lagrangian density corresponding to this model is obtained by adding to the SM Lagrangian density ($\mathcal{L}_{SM}$) the axion kinetic term ($\mathcal{L}_{axion\ kin}$) and the terms related to the axion interactions to both fermions and gauge bosons of the SM ($\mathcal{L}_{axion\ int}$) [12]:

$$\mathcal{L}_{eff} = \mathcal{L}_{SM} + \mathcal{L}_{axion\ kin} + \mathcal{L}_{axion\ int} \tag{1}$$

The kinetic term given below corresponds to the Lagrangian density of a free massive neutral scalar (labeled a). The axion mass is considered as a free parameter as long as it is less than the new physics energy scale Λ:

$$\mathcal{L}_{axion\ kin} = \frac{1}{2}\left[(\partial_\mu a)(\partial^\mu a) - m_a^2 aa\right] \tag{2}$$

The most general expression for the Lagrangian density describing the axion interactions arises from an Effective Field Theory (EFT), treating the axion as a pseudo-Nambu-Goldstone boson of an approximate global symmetry broken at a high-energy scale (labeled Λ in the following). In our framework, the EFT expansion in scale ratio is truncated at $1/\Lambda$ order. Therefore, the interactions are represented by dimension-5 (Lorentz- and SM-gauge-invariant) operators and the couplings by dimensionless scalar Wilson coefficients. Finally, the interaction terms can be expressed as:

$$\mathcal{L}_{axion\ int} = \frac{C_{aG}}{\Lambda}\mathcal{O}_{aG} + \frac{C_{aW}}{\Lambda}\mathcal{O}_{aW} + \frac{C_{aB}}{\Lambda}\mathcal{O}_{aB} + \frac{C_{a\Phi}}{\Lambda}\mathcal{O}_{a\Phi} + O\left(\frac{1}{\Lambda^2}\right) \tag{3}$$

with the dimension-5 operator definition:

$\mathcal{O}_{aG}$	$\mathcal{O}_{aW}$	$\mathcal{O}_{aB}$	$\mathcal{O}_{a\Phi}$
$aG^a_{\mu\nu}\tilde{G}^{a\mu\nu}$	$aW^a_{\mu\nu}\tilde{W}^{a\mu\nu}$	$aB_{\mu\nu}\tilde{B}^{\mu\nu}$	$i\left[\Phi^\dagger(\mathrm{D}_\mu\phi) - (\mathrm{D}_\mu\Phi^\dagger)\Phi\right]\partial_\mu a + \mathrm{h.c.}$

(4)

The coupling coefficients C_{aG}, C_{aW}, and C_{aB} correspond to the interaction magnitude between the axion and the SM gauge bosons. $G^a_{\mu\nu}$, $W^a_{\mu\nu}$, and $B_{\mu\nu}$ are respectively the field strength tensors related to $SU(3)_C$, $SU(2)_L$, and $U(1)_Y$. The tilde symbol $\sim$ depicts the dual of the field strength. Concerning the last term of the Lagrangian density, the $C_{a\Phi}$ coupling handles the interaction between the axion and the Higgs $SU(2)_L$ doublet Φ. The gauge invariant operator is made up of the axion, the Higgs field doublet (and its Hermitian conjugate), the (classical) derivative $\partial_\mu a$ and the (gauge-covariant) derivative $D_\mu\Phi$ of the Higgs doublet. The "h.c." refers to the Hermitian conjugate, ensuring that the Lagrangian density remains a real scalar (before quantization) and physically consistent. We notice that the four operators are Hermitian and therefore the Wilson coefficients are real scalar.

In the following, we will focus only the interaction terms containing $\mathcal{O}_{aV}$ operators. After the spontaneous symmetry breaking (SSB) of the gauge symmetry group $\mathrm{SU(2)_L} \times \mathrm{U(1)_Y}$ to $U(1)_{em}$, the Z^0, $W^\pm$, and γ bosons emerge from a mixing of gauge bosons and acquire masses except for the photon.

The interactions of the axion with these bosons are now described in terms of their corresponding field strengths $Z_{\mu\nu}$, $W^{\pm}_{\mu\nu}$ and $A_{\mu\nu}$, respectively:

$$\frac{C_{aW}}{\Lambda}\mathcal{O}_{aW} + \frac{C_{aB}}{\Lambda}\mathcal{O}_{aB} \quad \xrightarrow{EWSB} \quad \frac{\kappa_{a\gamma\gamma}}{\Lambda} a A_{\mu\nu}\tilde{A}^{\mu\nu} + \frac{\kappa_{aZZ}}{\Lambda} a Z_{\mu\nu}\tilde{Z}^{\mu\nu} + \frac{\kappa_{a\gamma Z}}{\Lambda} a A_{\mu\nu}\tilde{Z}^{\mu\nu} + \frac{C_{aW}}{\Lambda} a \left(W^{-}_{\mu\nu}\tilde{W}^{+\mu\nu} + W^{+}_{\mu\nu}\tilde{W}^{-\mu\nu} + \text{3-vector-boson terms}\right) \tag{5}$$

Here, $\kappa_{\mathrm{a}\gamma\gamma}$, κ_{aZZ}, and $\kappa_{\mathrm{a}\gamma\mathrm{Z}}$ represent the effective axion couplings to two photons, two Z^0 bosons, and mixed photon-Z states, respectively. The relationships between the post-SSB couplings and the original Wilson coefficients depend on the weark mixing angle θ_W and are given by the expression below.

$$\frac{\kappa_{a\gamma\gamma}}{\Lambda} = \frac{C_{aB}}{\Lambda}\cos^2\theta_W + \frac{C_{aW}}{\Lambda}\sin^2\theta_W, \tag{6}$$

$$\frac{\kappa_{aZZ}}{\Lambda} = \frac{C_{aB}}{\Lambda}\sin^2\theta_W + \frac{C_{aW}}{\Lambda}\cos^2\theta_W, \tag{7}$$

$$\frac{\kappa_{a\gamma Z}}{\Lambda} = 2\cos\theta_W\sin\theta_W\left(\frac{C_{aW}}{\Lambda} - \frac{C_{aB}}{\Lambda}\right) \tag{8}$$

These κ couplings are the one used in the Feynman rules and will help us to describe the different physical processes such as axion production and decay.

3 Motivated choice of the signal process

3.1 Axion production

At FCC-ee, the ALP can be produced classically, at Leading Order of the electroweak interaction, by assuming an ALP coupling to photon and/or Z boson. In the context of our theoretical framework, this process can be described by a non-null value of the $\kappa_{a\gamma Z}/\Lambda$ coupling. In this case, the e+ e- collision can lead to a (on-shell or off-shell) Z^0 boson which decays into an axion and a photon. Therefore the axion mass cannot exceed the mass of the Z^0 boson (the center of mass of the collision at FCC-ee) and it explains why the production of an axion and a Z^0 boson via an off-shell photon is kinematically forbidden. Besides, the coupling $\kappa_{a\gamma\gamma}$ can also lead to a final state made up of an axion and a photon. But this coupling is set voluntarily to 0 in order to avoid from an axion decay into a photon pair.

A non-null value of the $\kappa_{a\gamma Z}/\Lambda$ coupling allows the Z^0 boson to decay into an axion and a photon. As this decay channel has not been observed yet, this coupling is experimentally constrained by the measurement of the Z^0 total decay width, which is $2.4 \pm 2.3 \times 10^{-3}$GeV according to the Particle Data Group [13]. The experimental uncertainty on the total decay-width can be used as an upper limit on this exotic partial decay width. Taking into account the expression of the partial decay width, we obtain an upper limit on $\kappa_{a\gamma Z}/\Lambda$ which depends on the axion mass and coupling as we can see in the expression below:

$$\Gamma(Z \to \mathrm{a}\gamma) = \frac{(m_Z^2 - m_{ax}^2)^3}{6\pi m_Z^3}\left(\frac{\kappa_{\mathrm{a}\gamma\mathrm{Z}}}{\Lambda}\right)^2 \tag{9}$$

3.2 Axion decay

Within a model where the only enabled coupling is the $\kappa_{a\gamma Z}/\Lambda$ coupling, the axion is stable because the decay in the $Z^0\gamma$ final state is forbidden for the range of axion masses considered in this analysis. For dealing with an hadronic decay, we consider additionally a non-null value of the C_{aG}/Λ coupling which allows the axion to decay (in a gluon pair). We notice that this coupling does not have any impact on the axion production at FCC-ee. Besides, setting another coupling to a non-null value will have the consequence to add a branching ratio to the decay ax $\to$ gg.

After hadronization, the minimal final state content of this decay is a pair of pion as the pion is the lightest hadron of the Standard Model. This statement imposes a minimal value to the axion mass: 0.27 GeV. On contrary, if the axion mass is less than two times the pion mass, the axion can be considered as stable. At the detector level, produced hadrons can be reconstructed as jets by the CLD calorimeters. The number and the nature of these hadrons, and therefore the track multiplicity in the detector, will be typical of the axion mass value.

3.3 Case of a long-lived axion

It is relevant to mention that the produced axion can be also *long-lived*. By *long-lived* we mean the axion can reach (in average) the first layer of CLD detection before decaying. This phenomenon can give original experimental signatures such as *appearing tracks*, *displaced tracks*, *displaced vertices* or *displaced jets*. In order to identify the space parameter region where the axion is long-lived, the average flight distance of the axion in the laboratory frame $< d_{ax} >$ must be computed by using the total decay width (in our case the decay width related to the axion decay into gluons) and the axion boost. This distance must be less than about 50 cm in order to ensuring the track reconstruction with a reasonable efficiency. Beyond this threshold, the tracks coming from the axion decay products cannot be reconstructed and the axion could be considered as *invisible* (and could contribute to the missing energy).

The average flight distance $< d_{ax} >$ can be computed by the following formula:

$$< d_{ax} > = \frac{\hbar\beta\gamma}{\Gamma(\mathrm{ax} \to \mathrm{gg})}, \quad \text{with} \quad \Gamma(\mathrm{ax} \to \mathrm{gg}) = \frac{2}{\pi} m_{\mathrm{ax}}^3 \left(\frac{C_{aG}}{\Lambda}\right)^2 \quad \text{and} \quad \beta\gamma = \frac{\mathrm{s} - \mathrm{m}_{\mathrm{ax}}^2}{2\mathrm{m}_{\mathrm{ax}}\sqrt{\mathrm{s}}} \tag{10}$$

where $\beta\gamma$ is the Lorentz factor, c is the light velocity, and $\Gamma(\mathrm{ax} \to \mathrm{gg})$ is the axion decay width. Accordingly, the average flight distance $< d_{ax} >$ depends only on the axion mass and the C_{aG}/Λ coupling.

3.4 First exploration of the parameter space

The plot on the left in Figure 1 shows the production cross-section as a function of $\kappa_{a\gamma Z}/\Lambda$. The blank part represents the forbidden region due to the constraint on the Z total decay-width. We note that a 10 pb cross-secton is allowed for axion masses in the range of 0.3 GeV to 86 GeV.

The plot on the right in Figure 1 corresponds to the average flight distance $< d_{ax} >$ as function of the axion mass and the coupling. The dash line represents different values of flight distance: 0.1 cm, 1 cm, and 50 cm (threshold for reconstructing displaced tracks). We can conclude that the region of parameter space corresponding to a *long-lived* axion is contained between the first and the third dash lines.

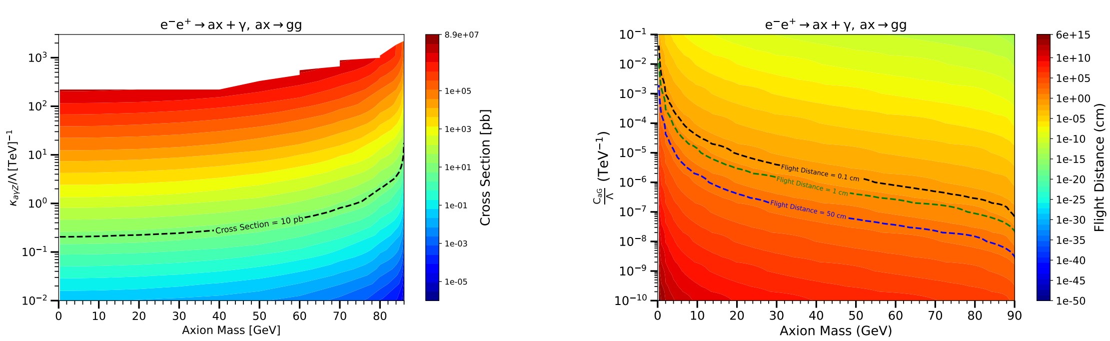

Figure 1: (left) Distributions of cross section as a function of $\kappa_{a\gamma Z}$ and axion mass, and (right) the flight distance as a function of C_{aG} and axion mass.

4 Sample generation and detector simulation

In the goal to achieve the sensibility study, signal and background samples of events must be produced. We remind that the signal consists in the axion production in association of a photon, followed by the axion decay into a pair of gluons. Concerning the background sources, the main SM process to take into account is the production of a photon and jets. For instance, the γ+2 jets background source has a cross-section of 225 pb. The jets correspond to the quark-antiquark pair produced by the Z boson where as the photo is coming from initial or final state radiation. To sum up, the Feynman diagrams for the signal and background processes are shown in the Figure 2.

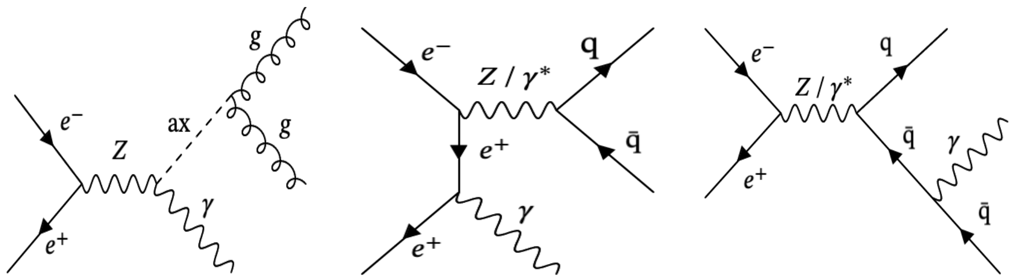

Figure 2: Feynman diagrams for the signal (left) and background processes (middle and right).

Background and signal events are both generated using the MadGraph5_aMC@NLO (MG) version 3.3.2 event generator [14]. This program is interfaced to the theoretical axion model [12] available in UFO (Universal FeynRules Output) [15, 16] format and produced by the framework FeynRules. The next step of the simulation is performed by using the Pythia8 [17] package which handles the initial and final states radiations, hadronisation, and hadron decays. Then, the detector simulation carried out by using the Delphes [18] framework, and for FCC-ee specific simulations, the fast simulation card, FCC-eeDetWithSiTracking, is used. Finally, the event selection for the sensitivity analysis is performed using MadAnalysis5_v1.9.60 framework [19].

Many signal samples have been generated for covering the region parameter space. Indeed, signal events are generated for different axion masses ranging from 0.3 GeV to 86 GeV, with photon transverse momentum $\mathrm{p_T} \geq$ 5 GeV and a jet transverse momentum $\mathrm{p_T} \geq$ 1 GeV. The parameter space for the couplings C_{aG}/Λ and $\kappa_{a\gamma Z}/\Lambda$ is scanned over a wide range from 10^{-9} to 1 TeV^{-1}. For each signal sample, one million of events are generated, whereas 20 millions events are produced for the background processes.

5 Analysis and results

5.1 Reconstruction and event selection

The signal final state in this analysis consists of one photon and exactly two jets, where the jets originate from the axion decay. The several kinematic observables are studied to maximize the discrimination between axion signals and the SM background. At the reconstruction level, key observables include the $\mathrm{p_T}$ of the photon and jets and the invariant mass of the jet pair. In particular, the $\mathrm{e^-e^+}$-Durham $\mathrm{k_T}$ algorithm with exclusive clustering is applied, and events are required to have exactly three jets $\mathrm{N_{jets}}$ =3 to effectively identify axion-induced jet signatures. After selecting photons with $p_\mathrm{T} > 15$ GeV, which are reconstructed as jets, these jets are removed from the event if they satisfy $\Delta R(\text{jets}, \gamma) > 0.5$. The ΔR represents the distance between a photon and a jet in the detector's pseudorapidity-azimuthal (η, ϕ) space.

The final selection for sensitivity analysis requires a leading photon with p_T >15 GeV and leading and subleading jets with p_T >8 GeV, ensuring a well-defined and high-purity final state. To further suppress background contributions, a dijet invariant mass cut is applied, with the mass selected within a range defined by the axion mass and a corresponding mass window cut. The dijet invariant mass is reconstructed using the leading and subleading jets, and the mass window is decided based on the axion mass, with values set to 0.5, 4, 6, and 10 GeV for axion masses below 1, 10, 30, and 90 GeV, respectively.

The signal and background processes are normalised to an integrated luminosity of 125 ab^{-1}. This scaling ensures that the expected number of events reflects real experimental conditions. Figure 3 shows the invariant mass distributions of the leading and subleading jets after the selection of the γ + 2 jets. These distributions are shown for a representative coupling $\kappa_{a\gamma Z}$=0.33 (or C_{aW}= 0.3), $\kappa_{a\gamma Z}$=1.1 (or C_{aW}= 1), $\kappa_{a\gamma Z}$=2 (or C_{aW}=2.2) and various values C_{aG} that correspond to different flight distances of axion decay within the tracker volume (0–50 cm). These distributions illustrate the impact of different signal masses and background processes on the reconstructed jet mass spectra.

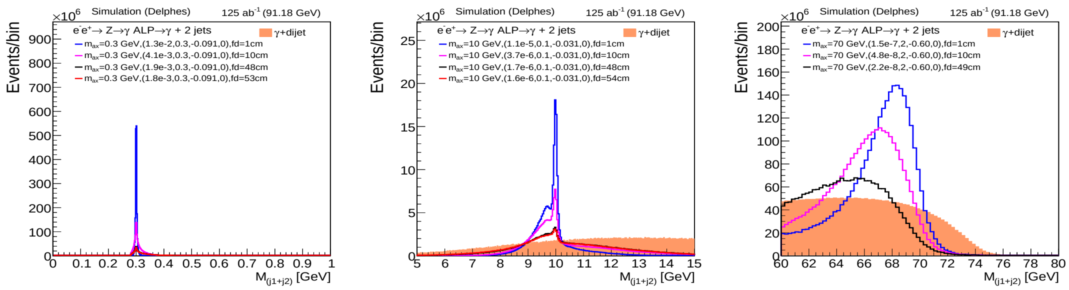

Figure 3: Distributions of the dijet invariant mass after event selection requiring γ + 2 jets, for axion masses of 0.3 GeV ($\kappa_{a\gamma Z}$ = 0.33 or C_{aW}= 0.3) left, 10 GeV ($\kappa_{a\gamma Z}$ = 1.1 or C_{aW}= 1) middle, and 70 GeV ($\kappa_{a\gamma Z}$ = 2 or C_{aW}= 2.2) right, respectively.

5.2 Sensitivity study

Events are selected with $p_{\rm T}$ > 15 GeV for the leading photon, $p_{\rm T}$ > 8 GeV for the leading and subleading jets, along with the applied dijet invariant mass cut as mentioned in Subsection 5.1. The sensitivity (S) for each benchmark point is calculated using the formula S= $n_s/\sqrt{n_s + n_b}$, where n_s and n_b represent the expected number of signal and background events, respectively. A higher sensitivity value indicates better discrimination of the ALP signal from the background.

Sensitivity trends are further illustrated in Figure 4. The plot on the top of the figure shows the sensitivity as a function of axion mass, with each curve corresponding to a different flight distance. The plot on the bottom displays sensitivity as a function of $\kappa_{a\gamma Z}$ for various flight distances, where the colors denote the different axion masses and the line styles represent the different flight distances. In the bottom plot, the red dotted horizontal line represents the 3σ sensitivity threshold. Overall, this analysis provides valuable insight into how different ALP parameter choices influence event kinematics and helps optimize the selection criteria for enhanced sensitivity in future FCC-ee experiments.

6 Reinterpretation scheme for the analysis results

6.1 Reinterpretation in terms of Wilson coefficients

The analysis has been performed with the hypothesis of a null $\kappa_{a\gamma\gamma}/\Lambda$ coupling and an upper limit has been set to $|\kappa_{a\gamma Z}/\Lambda|$. These two anomalous couplings can be expressed as a linear combination of Wilson coefficient as it is precised by Equation 8. By reversing the equation, the limit on $|\kappa_{a\gamma Z}/\Lambda|$ can be transposed on $|C_{aB}/\Lambda|$ and $|C_{aW}/\Lambda|$:

$$\frac{\kappa_{a\gamma Z}}{\Lambda} = 2\frac{\cos^3\theta_W}{\sin\theta_W}\frac{C_{aW}}{\Lambda} = -2\frac{\cos^5\theta_W}{\sin^3\theta_W}\frac{C_{aB}}{\Lambda} \tag{11}$$

$$\frac{C_{aB}}{\Lambda} = -\tan^2\theta_W\frac{C_{aW}}{\Lambda} \tag{12}$$

6.2 Extension to $\kappa_{a\gamma\gamma}/\Lambda \neq 0$

If $\kappa_{a\gamma\gamma}/\Lambda \neq 0$, the relation between C_{aB}/Λ and C_{aW}/Λ is not valid anymore. We would like to extend the analysis results to the case of small value of $\kappa_{a\gamma\gamma}/\Lambda$ with respect to $\kappa_{a\gamma Z}/\Lambda$. We reserve the case

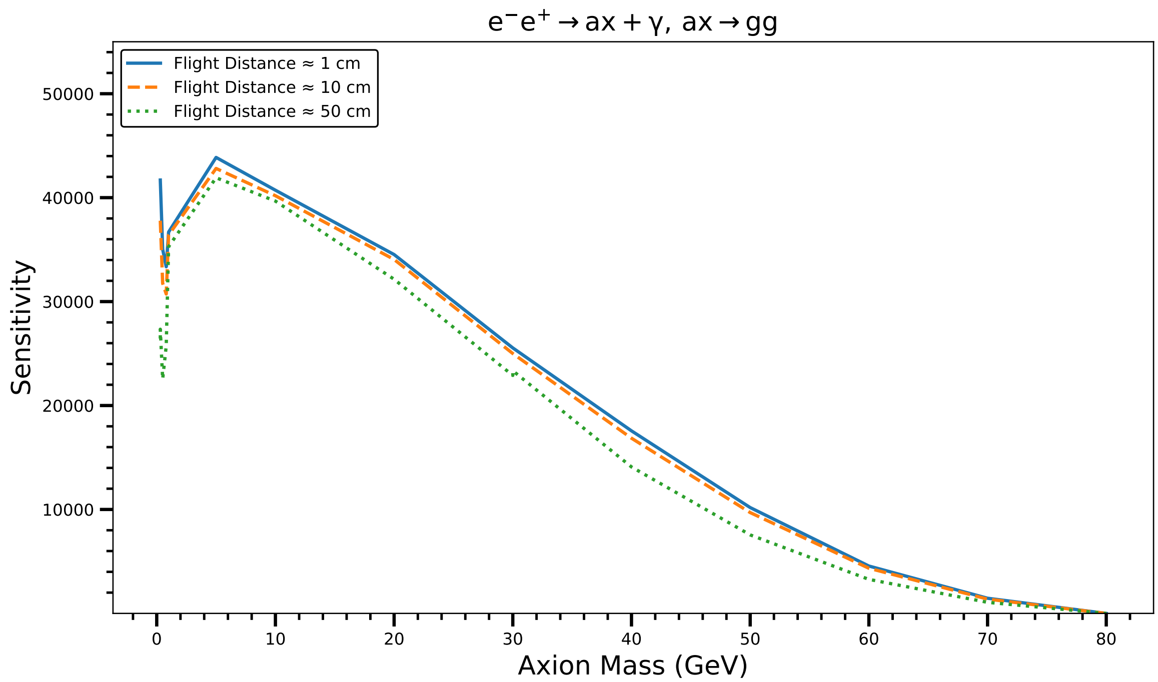

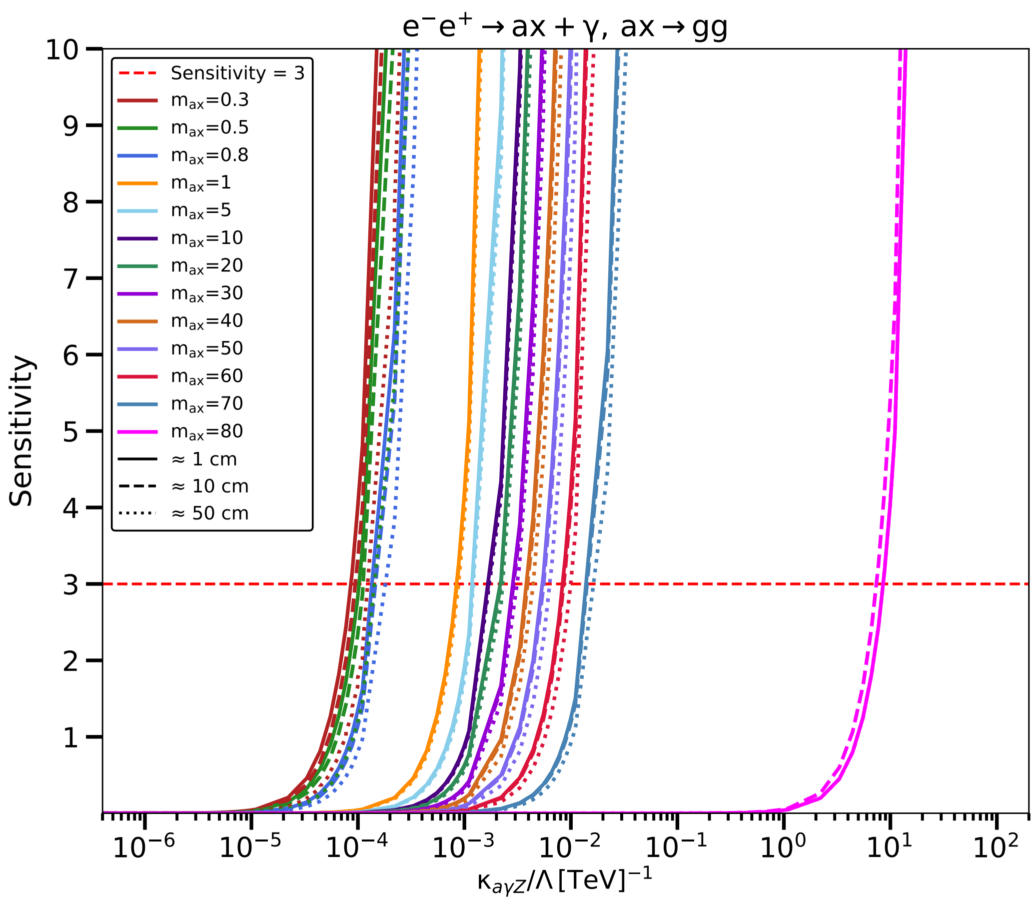

Figure 4: Distributions of sensitivity as a function of axion mass for fixed $\kappa_{a\gamma Z}$=0.33 (C_{aW}= 0.3) (top) and sensitivity as a function of $\kappa_{a\gamma Z}$ for different flight distances (bottom).

of large values for the analysis $ax \to \gamma\gamma$.

Avoiding from designing a new analysis, the aim of a reinterpretation study could be the estimation of the range of $\kappa_{a\gamma\gamma}/\Lambda$ values for which the previous results are still valid. Guidelines for reinterpreting the results in this scenario:

- A new physical process contributes to the production of an axion associated to a photon via a γ^*. The cross-section calculation must take into account this process and its interference with the process involving $\kappa_{a\gamma Z}$ (the sign of the interference is given by the sign of the product $\kappa_{a\gamma\gamma} \times \kappa_{a\gamma Z}$). If the $\kappa_{a\gamma\gamma}$ is small enough, this new contribution can be negligible.
- In the narrow-width approximation of the Breit-Wigner, the presence of the decay channel $ax \to \gamma\gamma$ can be taken into account by specifying a branching ratio not equal to 100% to the decay $ax \to gg$. It is remarkable that the branching ratio depends only on the coupling ratio $\kappa_{a\gamma\gamma}/\kappa_{a\gamma Z}$ and not on the axion mass.
- The exploration of parameter space region where the axion is long-lived must also consider the fact that $\kappa_{a\gamma\gamma}/\Lambda$ changes the total decay width and therefore the average flight distance $< d_{ax} >$. Analysis results can be still valid if the $\kappa_{a\gamma\gamma}/\Lambda$ is very small, for instance a $BR(ax \to \gamma\gamma) < 0.1\%$.

7 Conclusion

This study presents an initial fast simulation-based sensitivity analysis for Axion-Like Particles (ALPs) at FCC-ee, focusing on the production of a single axion in association with a photon, where the axion subsequently decays into a pair of gluons. Signal and background samples were generated using a suite of software packages (containing especially FeynRules, MadGraph_aMC@NLO and Delphes) and a sensitivity analysis was designed and implemented within the MadAnalysis framework. The results indicate a promising reach in the parameter space of ALP-gluon couplings, highlighting capability of FCC-ee to probe new physics. The decay length has not yet been considered in this analysis. A more detailed study, including displaced vertex reconstruction and multivariate analysis techniques, will be essential for a complete evaluation of the ALP parameter space. Future studies incorporating full detector simulation and systematic uncertainties are expected to further refine these findings, providing a more comprehensive assessment of FCC-ee discovery potential. Some guidelines are provided in order to reinterpret the produced the results to an extension of the theoretical assumptions used. The presented analysis is still work in progress, and further improvements on event selection and signal extraction are being investigated. In particular important handles to improve the signal to background ratio have not been exploited yet.

References

[1] R. D. Peccei and H. R. Quinn. “CP conservation in the presence of pseudoparticles”. Phys. Rev. Lett. 38 (1977), pp. 1440–1443.

[2] R. D. Peccei and H. R. Quinn. “Constraints imposed by CP conservation in the presence of pseudoparticles”. Phys. Rev. D 16 (1977), pp. 1791–1797.

[3] S. Weinberg. “A new light Boson?” Phys. Rev. Lett. 40 (1978), pp. 223–226.

[4] F. Wilczek. “Problem of strong P and T invariance in the presence of instantons”. Phys. Rev. Lett. 40 (1978), pp. 279–282.

[5] J. Alimena et al. “Searching for long-lived particles beyond the standard model at the Large Hadron Collider”. J. Phys. G: Nucl. Part. Phys 4 (2020).

[6] E. S. Group. “2020 Update of the European strategy for particle physics (brochure)”. Tech Rep Cern-esu-015 (2020). CERN, Geneva.

[7] F. Collaboration. “FCC-ee: The Lepton Collider: Future Circular Collider conceptual design report volume 2”. Eur. Phys. J. Spec. Top. 228 (2019).

[8] M. Chrzaszcz, R. G. Suarez, and S. Monteil. “Hunt for rare processes and long-lived particles at FCC-ee”. Eur. Phys. J. Plus. 136 (2021).

[9] C. B. Verhaaren et al. "Searches for long-lived particles at the future FCC-ee". Front. Phys. 10 (2022).

[10] M. Bauer, M. Neubert, and A. Thamm. "Collider probes of Axion-like particles". JHEP 2017 (2017).

[11] M. Bauer et al. "Axion-like particles at future colliders". Eur.Phys.J.C 79 (2019).

[12] I. Brivio and M. B. e. a. Gavela. "ALPs effective field theory and collider signatures". Eur.Phys.J.C 77 (2017), p. 572.

[13] R. L. Workman et al. "Review of Particle Physics". PTEP 2022 (2022), p. 083C01.

[14] J. Alwall et al. "The automated computation of tree-level and next-to-leading order differential cross sections, and their matching to parton shower simulations". JHEP 2014 (2014).

[15] C. Degrande et al. "UFO – The Universal FeynRules Output". Comput. Phys. Commun. 183 (2012), pp. 1201–1214.

[16] L. Darmé et al. "UFO 2.0: the 'Universal Feynman Output' format". Eur.Phys.J.C 83 (2023).

[17] C. Bierlich et al. "A comprehensive guide to the physics and usage of PYTHIA 8.3". (2022). arXiv: 2203.11601 [hep-ph].

[18] J. de Favereau et al. "DELPHES 3: a modular framework for fast simulation of a generic collider experiment". JHEP 2014 (2014).

[19] J. Y. Araz, B. Fuks, and G. Polykratis. "Simplified fast detector simulation in MADANALYSIS 5". Eur. Phys. J. C 81 (2021).